Effect of Hydrogen Concentration on Nanoindentation Softening and Hardening in Iron: Ferrite Phase of S25C and Single-crystal Fe-3wt.%Si

Shinya TAKETOMI,[1]* Toshiki TANIGUCHI,[1] Hiroki YAMAMOTO,[1] Seiya HAGIHARA,[1] Sadahiro TSUREKAWA[2] and Ryosuke MATSUMOTO[3]

1) Department of Mechanical Engineering, Saga University, 1 Honjo-machi, Saga, 840-8502 Japan.
2) Division of Materials Science and Chemistry, Faculty of Advanced Science and Technology, Kumamoto University, 2-39-1 Kurokami, Kumamoto, 860-8555 Japan.
3) Faculty of Engineering, Kyoto University of Advanced Science, 18 Yamanouchi Gotanda-cho, Ukyo-ku, Kyoto, 615-8577 Japan.

Plastic deformation is key to understanding hydrogen embrittlement in steels. Although macroscopic to microscopic observations and analyses have reported softening and hardening behavior in the presence of hydrogen, the mechanisms causing these effects and the overall mechanisms remain unclear. Therefore, this study applies nanoindentation tests to the ferrite phase of bcc-structured polycrystalline carbon steel S25C and single-crystalline iron with 3 wt.% silicon (Fe-3wt.%Si). The change in indentation work is evaluated by varying the exposure time in air between the uncharged and hydrogen-charged materials, focusing on the hydrogen concentration. The change in work per unit indentation volume caused by hydrogen (hydrogen-induced work) is investigated, revealing that the specimens harden immediately upon hydrogen charging, and then gradually soften with increasing exposure time before returning to their original state. This variation is attributed to the change in hydrogen concentration. The softening and hardening behavior with and without hydrogen, as confirmed by nanoindentation tests, is suggested to quantitatively affect the macroscopic mechanical response, which is determined by the mobility of screw dislocations in these materials.

KEY WORDS: hydrogen embrittlement; nanoindentation; softening and hardening; hydrogen concentration; dislocation mobility.

1. Introduction

Hydrogen embrittlement has become a major issue in the strengthening of steels and the expansion of their use in hydrogen-intruding environments. Although long-term studies have been performed on the mechanism of hydrogen embrittlement, many parts of the overall picture remain unresolved and are still being investigated, with plastic deformation being key to understanding the hydrogen-embrittlement mechanism and its development in steels. Nevertheless, conflicting results have been reported on how hydrogen affects macroscopic plastic deformation, *e.g.*, the stress–strain relationship of pure iron has been reported to both soften[1] and harden[1,2] upon electrochemical hydrogen charging. The softening or hardening of macroscopic plasticity is considered to strongly depends on the fundamental process of dislocation motion. In microscopic observations of dislocation motion, the effect of hydrogen on individual cases of dislocation motion has been investigated using transmission electron microscopy (TEM).[3,4] It has been reported that the distance between dislocations (edge, screw and mixed dislocations) decreases with hydrogen introduction in a variety of materials. However, our molecular dynamics analysis using α-iron suggests that when the specimen size is extremely small, screw dislocations move due to changes in surface energy caused by hydrogen atoms adsorbed on the surface steps,[5] and the results of dislocation motion in TEM experiments cannot be said to directly correspond macroscopic softening in bulk materials. On the other hand, our molecular statics analysis indicates that the mobility of the $1/2\langle 111\rangle\{112\}$ edge dislocation in α-iron transitions from hardening to softening with decreasing hydrogen concentration.[6,7] Softening, which increases dislocation mobility, only occurs under extremely low hydro-

* Corresponding author: E-mail: taketomi@me.saga-u.ac.jp

gen concentrations. However, in a result that differs from the aforementioned results of molecular statics analysis, a long-time molecular dynamics analysis using the same edge-dislocation model indicates that hardening occurs with decreasing dislocation mobility even at extremely low hydrogen concentrations,[8] and this is explained by the fact that analyzing slow dislocation velocities are still difficult, and identifying variations in stress are also difficult because the stress required to move edge dislocations becomes very small at low dislocation velocities. On the other hand, the results of first-principles calculations by Itakura *et al.*[9] indicate that the mobility of screw dislocations in α iron goes from low to high depending on the hydrogen concentration. The edge dislocations are extremely mobile in bcc-structured steels, and the screw dislocations significantly affect plasticity. Therefore, a long-term analysis of screw-dislocation motion can provide direct observation of the time evolution for screw dislocation motion and hydrogen diffusion. However, such analyses remain difficult owing to their high computational cost and the validity of analyses of screw-dislocation motion.

Nanoindentation methods have attracted attention as a method to investigate the development of microscopic failure in materials. In nanoindentation testing, a microindenter is pressed into a material to obtain the time variation of test force and the indentation depth. Nanoindentation testing also reveals the mechanical properties of materials. Recently, this method has been used to study hydrogen embrittlement. For example, Nagashima *et al.*[10] applied nanoindentation to investigate the ferrite microstructure of steel and reported that due to enhanced dislocation emission, pop-in loading decreases in hydrogen-charged materials, whereas hydrogen charging causes no effect in steels with reduced vacancy densities. Barnoush *et al.* performed a series of studies using electrochemical nanoindentation techniques[11] and reveal that hydrogen-enhanced homogeneous dislocation nucleation reduces pop-in loading in various metals, which attribute the decrease in shear modulus, dislocation line energy, and stacking-fault energy.[12,13] In other research on hydrogen-induced softening and hardening phenomena, Lee *et al.* reported that the hardness of steel softened or hardened depend on indenter tip blunting.[14] Tomatsu *et al.*[15] applied electrochemical nanoindentation tests on various pure heat-treated irons and reported that softening occurs at lower indentation speed in materials with high dislocation density, and also reported that hydrogen trapped in the vicinity of dislocations suppresses work hardening and softening occurs due to increased dislocation mobility. Zhao *et al.*[16] conducted nanoindentation tests on steels and reported that the nanohardness transitions from hardening to softening depend on the hydrogen-charging method (hardening occurs upon electrochemical charging and softening upon gas charging). Furthermore, a comparison of the hardness distribution in the thickness direction of the electrochemically charged specimens showed that hardening occurs at the surface but softening occurs in the inner part of the plate. They concluded that hydrogen concentration and hydrogen concentration gradients influence the softening and hardening of steel.

The present study applies nanoindentation tests to the ferrite phase of polycrystalline S25C carbon steel and to single-crystalline Fe-3wt.%Si, with the plastic deformation behavior of small volumes being investigated using small indentation depths, and the work per unit indentation volume being investigated in the relatively early stages of plastic deformation when individual dislocations exert a significant influence. This study aims to clarify how hydrogen concentration affects the microscopic plastic deformation of the bcc ferrite phase. This is done via experiments in which the exposure time to air was varied after hydrogen charging. This was achieved using the same specimens with the same hydrogen-charging method but with different hydrogen concentrations.

2. Experimental Method

2.1. Material

This study used polycrystalline carbon steel S25C and Fe-3wt.%Si coarse-grained material. Carbon steel S25C specimens with a length of 20.0 mm, a plate width of 5.0 mm, and a thickness of 0.5 mm were prepared from commercially available bars, and Fe-3wt.%Si single-crystal specimens with a length of 22.0 mm, a plate width of 16.0 mm, and a thickness of 2.0 mm were made from coarse-grained material. Both specimens were made from the as-received materials with no additional heat treatments. The measurement surface into which the indenter was pressed in the nanoindentation test was initially wet polished sequentially with #400, #800, #1500, and #2000 emery paper, followed by buffing with a 1.0-μm alumina suspension. After polishing, the carbon steel S25C was etched using a 3% Nital solution (97% ethanol, 3% nitric acid). An Optical micrograph of the microstructure of the specimens is shown in **Fig. 1**, and nanoindentation was carried out on the ferrite phase of S25C. Here, our preliminary tests on the ferrite phase of the non-etched specimens showed almost similar load–displacement curves compared to the etched ferrite phase, so the influence of the corrosion layer is considered to be negligible. Conversely, the back-reflection Laue method was used to identify the crystallographic orientation of Fe-3wt.%Si. **Figure 2** shows the Laue pattern, where, as identified from the Laue spots, the crystal orientation normal to the surface was close to the <100> axis. Figure 2 shows a stereo projection of the specimen normal to the surface.
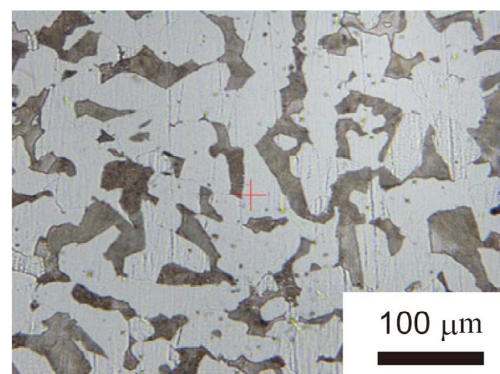

Fig. 1. Crystal structure of S25C after etching as observed by optical microscopy. White (black) grains represent the ferrite (pearlite) phase. (Online version in color.)
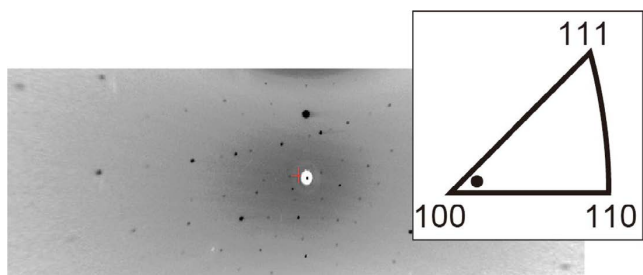
Fig. 2. Laue pattern of Fe-3wt.%Si obtained using the back-reflection Laue method. The normal direction of the specimen is depicted by stereo projection. (Online version in color.)
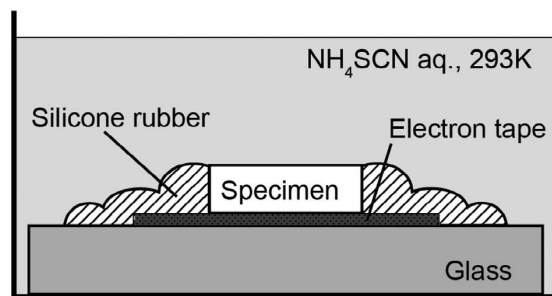

Fig. 3. Schematic of hydrogen-charging setup. The polished measurement surface is covered to prevent corrosion during hydrogen charging. The setup is maintained at 20°C for 24 h while charging.

2.2. Hydrogen Charging

In this study, to prevent the measurement surface from corrosion during hydrogen charging, the polished surface was protected with electron tape (Tsukasa Trading), with the tape surface attached to the glass, as per the method of Nagashima et al.,[10] with specimens being immersed in ammonium thiocyanate (NH_4SCN) solution (0.1 mol/L). The back surface of the specimen was polished with #400 emery paper before hydrogen charging to unify the roughness of the charging surfaces, with the sides of the specimens being covered with silicone rubber to prevent the solution from penetrating. The sample was then immersed in 50 ml of NH_4SCN solution and maintained at 20°C for 24 h. **Figure 3** shows a schematic of the hydrogen-charging setup. Hydrogen is charged only on the side opposite to the polished surface and in contact with the solution but penetrates sufficiently into the material because it has a bcc structure with extremely high diffusion coefficient and thin plate thickness (0.5 mm for S25C and 2.0 mm for Fe-3wt.%Si). After hydrogen charging, the specimens were polished with #400 emery paper to remove corrosion products adhering to the back surface. The glass and electron tape were removed, the measuring surface was cleaned with ethanol, and the sample was exposed to air for 30 min after hydrogen charging to standardize the test start time before starting the experiment. To vary the hydrogen concentration in the sample, the exposure time of the specimen was set to 0 h, with the experiment starting 30 min after hydrogen charging, and the hydrogen concentration then being changed by exposing the sample to air at 20°C, with a maximum exposure time of 216 h.

2.3. Nanoindentation Testing and Evaluation

Indentation tests were performed using a Shimadzu DUH-211S dynamic micro hardness tester. A 115° triangular pyramidal indenter was used as the indenter (see **Fig. 4**). To assess how hydrogen affects the initial state of plastic deformation, the indentation depth was set to 50 nm. The indentation rate was 0.015 mN/s (approximately 2.0 nm/s). In material evaluation tests using the nanoindentation method, experimental accuracy and reproducibility must be ensured. To this end, this study conducted five nanoindentation tests at different locations on the same ferrite-phase of carbon steel S25C specimen to form one set of measurements, with each set of experiments being performed on different grains to avoid excessive indentation tests on a single grain. Three sets of nanoindentation tests were conducted on the no-hydrogen charged material, three sets each on the
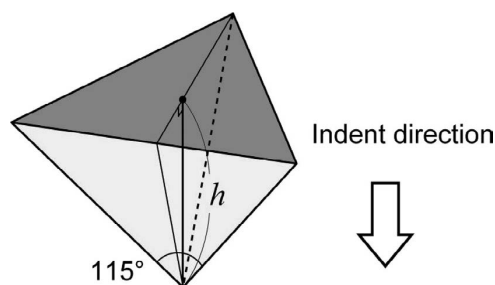

Fig. 4. Ideal geometry of a 115° triangular pyramidal indenter.

material exposed to air for 0, 24, and 48 h after hydrogen charging, two sets each on the material exposed for 72, 96, 120, and 144 h, and one set on the material exposed for 216 h. The number of experimental sets for each exposure time is referred to as X_H hereafter. For Fe-3wt.%Si, one set of 10 tests was conducted on samples exposed for 0, 24, 48, 72, 96, and 168 h. Each of these sets of experiments taking a few hours, and thermal drift increasing as the test time increased.[15] In this study, the windshield covering the experimental setup was covered with Styrofoam to minimize temperature fluctuations during the experiments. Furthermore, the influence of external micro-vibrations was reduced by installing the apparatus on an active table-top vibration isolator.

Hardness is one of the parameters that describes the mechanical properties of a material and is treated as a specific physical property that represents macroscopic material properties. Several engineering definitions of hardness exist; however, most hardness values applicable to steels are obtained by indenting an indenter into the material surface and dividing the indentation load by the surface area of the indentation. When the indentation load is F and the indentation depth is h, the engineering hardness H is generally expressed as:

$$H = A\frac{F}{Bh^2} \quad\quad\quad\quad\quad\quad (1)$$

where A is a constant determined by the hardness definition and B, which is determined by the indenter geometry, is a conversion factor between indentation depth and surface area. As hardness is a constant physical property, the macroscopic indentation load is defined as a quadratic function of the indentation depth. The indentation work W done by the indenter is obtained by integrating the indentation load F over the indentation depth h so that the indentation work is

a cubic function of the indentation depth h. The indentation volume of the indenter is also a cubic function of h. Therefore, the macroscopically measured hardness is qualitatively proportional to the indentation work per unit indentation volume of the indenter.

Conversely, for the elastic deformation occurring during the initial indentation process, using Hertzian elastic contact, the indentation load F is expressed as follows:

$$F = \frac{4}{3}E^* R^{\frac{1}{2}} h^{\frac{3}{2}} \quad \text{.............................. (2)}$$

where R is the radius of the spherical indenter, h is the indentation depth, and E^* is the reduced modulus of elasticity calculated as follows from the modulus of each body:

$$\frac{1}{E^*} = \frac{1-\nu_1^2}{E_1} + \frac{1-\nu_2^2}{E_2} \quad \text{....................... (3)}$$

The subscripts 1 and 2 refer to the indenter and the specimen, E is the elastic constant, and ν is Poisson's ratio. Here, the geometry of the indenter differs from our experiments, however, the small volume indentation test is not considered to make much difference due to the geometry of the indenter. Usually, in nanoindentation tests, E^* and R are constants, so Eq. (2) is simplified using the constant α as follows:

$$F = \alpha h^{\frac{3}{2}}$$
$$\alpha = \frac{4}{3}E^* R^{\frac{1}{2}} \quad \text{................................ (4)}$$

Thus, according to the Hertzian elastic contact theory, the indentation load is a 3/2-order function of the indentation depth. In nanoindentation tests, the indentation load is considered to changes from a 3/2- to a 2nd-order function as the indentation depth increases. In nanoindentation tests, the 3/2-order function based on Hertzian elastic contact theory well reproduces the load–displacement relationship.[13] As a preliminary investigation, the load–displacement relationship obtained from the nanoindentation test was approximated using 3/2- and 2nd-order functions. In the end, the 3/2-order function is used because it better reproduces the experimental results. Although the nanoindentation tests reported herein are considered to depend strongly on elastic deformation due to the small indentation depth, the physical meaning of α differs from that of Eq. (4) because the experiment also includes plastic processes. The hydrogen-induced load ΔF is

$$\Delta F = \left(\alpha_{\text{with H}} - \alpha_{\text{w/o H}}\right) h^{\frac{3}{2}} \quad \text{..................... (5)}$$

where $\alpha_{\text{w/o H}}$ ($\alpha_{\text{with H}}$) is the constant α in the absence (presence) of hydrogen charging. Integrating ΔF over the indentation depth h gives the change ΔW in indentation work due to hydrogen charging (i.e., the hydrogen-induced work). The result is as follows:

$$\Delta W = \frac{2}{5}\left(\alpha_{\text{with H}} - \alpha_{\text{w/o H}}\right) h^{\frac{5}{2}} \quad \text{................... (6)}$$

The indenter's indentation volume V is

$$V = \beta h^3, \quad \text{................................ (7)}$$

where β is a constant determined by the indenter geometry. The ideal geometry of a 115° triangular pyramidal indenter used in this study is shown in Fig. 4. From geometrical calculations based on this geometry, β is

$$\beta = \frac{\sqrt{3}\sin^2(57.5°)}{3-4\sin^2(57.5°)} = 7.96 \quad \text{.................. (8)}$$

Finally, the hydrogen-induced work per unit indentation volume is

$$\Delta H = \frac{\Delta W}{V} = \frac{2\left(\alpha_{\text{with H}} - \alpha_{\text{w/o H}}\right)}{5\beta\sqrt{h}} \quad \text{................ (9)}$$

3. Experimental Results

Figures 5(a)–5(c) and 5(d)–5(f) show the load–displacement relationship obtained from the nanoindentation tests for S25C and Fe-3wt.%Si, respectively. Figures 5(a) and 5(d) show the results for the no hydrogen charged case, Figs. 5(b) and 5(e) show the results for 0 h after hydrogen charging, and Figs. 5(c) and 5(f) show the results for 48 h of exposure to air after hydrogen charging. The gray and green curves show the loading data for one set of experiments, and the least-square fits to Eq. (4) are the black-dashed (red) lines for the no hydrogen-charged material. The residuals of loading were determined from the experimental data and approximate curves, and the standard deviations for each experimental set were found to be a minimum of 0.017 mN and a maximum of 0.048 mN for S25C and a minimum of 0.021 mN and a maximum of 0.032 mN for Fe-3wt.%Si. Therefore, it can be said that the fits using the 3/2-order function reproduce the experimental data relatively well. Here, the experimental setup used in this study does not allow distinct pop-in phenomena to be observed. **Figure 6** shows the hydrogen-induced indentation loads obtained using Eq. (5). For both S25C and Fe-3wt.%Si, the indentation load peaks at 0 h after hydrogen charging. As the exposure time increases, the hydrogen-induced load gradually becomes negative, with the minimum reached after 72 h for S25C and 48 h for Fe-3wt.%Si. As the exposure time increases further, the hydrogen-induced load almost reaches zero.

Figure 7 summarizes the hydrogen-induced work per unit indentation volume as a function of exposure time to air according to Eq. (9). The results are summarized for different indentation depths [10–50 nm substituted into Eq. (9)]. The hydrogen-induced work per unit indentation volume is evaluated from three sets of hydrogen un-charged S25C and X_H sets (described in section 2.3.) of charged specimen for each exposure time. An averaged value from totally $3X_H$ of combination for different exposure time are shown. For Fe-3wt.%Si, the results of a single set were used in the calculation. The work per unit volume is greatest for all materials at 0 h after hydrogen charging. Furthermore, upon increasing the exposure time to air, the work per unit indentation volume decreases as the material softens; however, after further exposure to air, the work per unit indentation volume returns to the same level as for the un-charged condition. With increasing indentation depth, the indentation work per unit
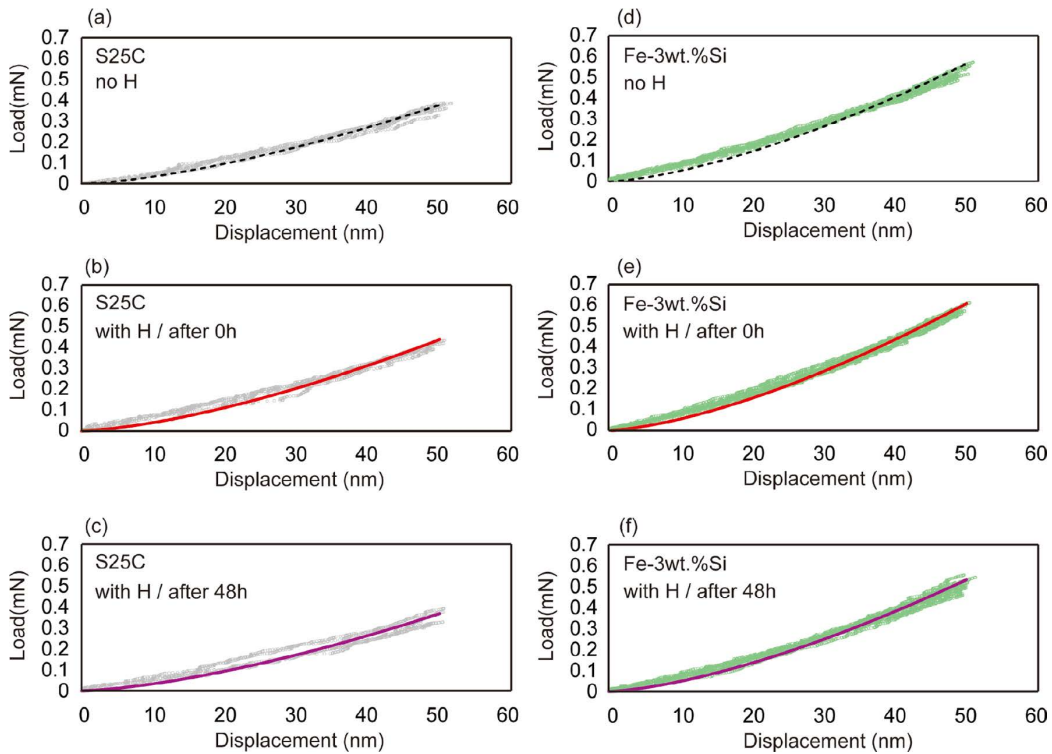
Fig. 5. Load as a function of displacement during nanoindentation tests. (a)–(c) Results for S25C steel without hydrogen charge, immediately after hydrogen charging, and exposed to air for 48 h after hydrogen charging, respectively. (d)–(f) Results for Fe-3wt.%Si without hydrogen charging, immediately after hydrogen charging, and exposed to air for 48 h after charging respectively. Red solid lines in the figures are approximated curve fitted by Hetrzian elastic contact theory. (Online version in color.)
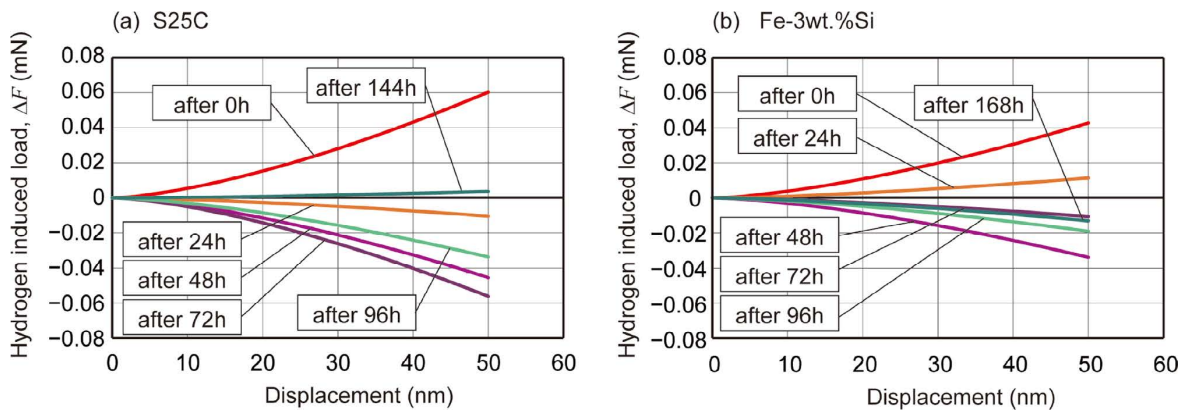

Fig. 6. Hydrogen-induced load as a function of displacement for (a) S25C and (b) Fe-3wt.%Si. The hydrogen-induced load is defined by the difference between the approximate load curve with hydrogen and that without hydrogen under the conditions of Fig. 5. (Online version in color.)
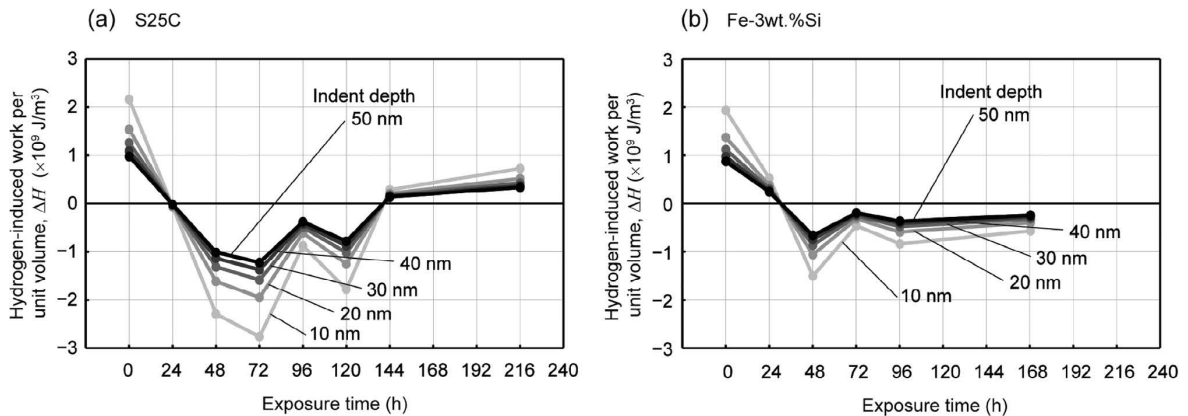

Fig. 7. Hydrogen-induced work per unit indentation volume as a function of time exposed to air for (a) S25C and (b) Fe-3wt.%Si. Equation (9) was used to calculate the curves for indentation depths of 10–50 nm.
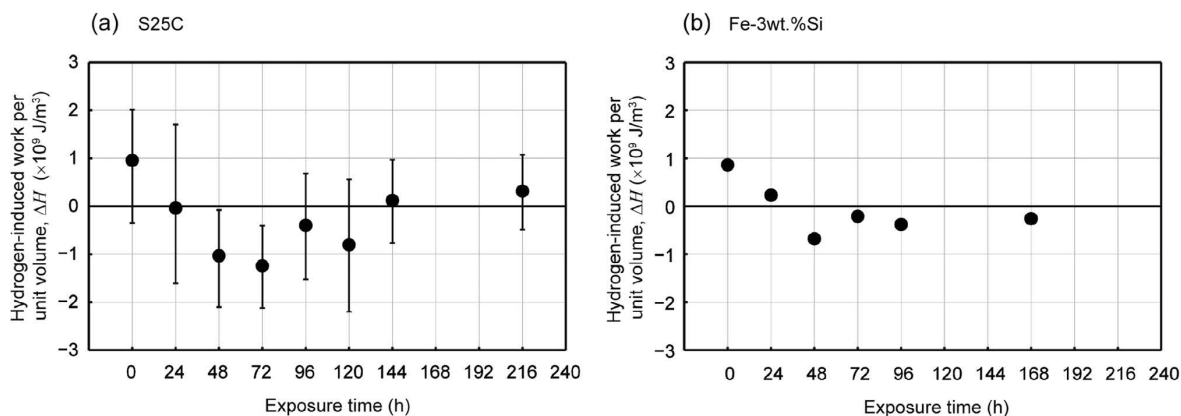
(a) S25C (b) Fe-3wt.%Si

Fig. 8. Hydrogen-induced work per unit indentation volume as a function of time exposed to air for (a) S25C and (b) Fe-3wt.%Si. The indent depth is 50 nm for both specimens. The dots in (a) give the average for different experimental sets. The results for polycrystalline S25C vary because of the different ferrite phases. The maximum and minimum work is indicated by the error bars.

indentation volume converge. This result is explained by Eq. (9), which goes to zero as the indentation depth h increases. This tendency is inevitable when the order of the polynomial approximation of the indentation load F as a function of indentation depth h is less than two and is presumably due to the elastic properties of the material, as discussed in Section 2.3. For example, **Fig. 8** shows the hydrogen-induced work per unit indentation volume as a function of exposure time and for an indentation depth of 50 nm. Here, the results for S25C are compared for different ferrite phases, showing that the variation depends on the crystallographic orientation. Both materials reveal a hardening–softening transition with increasing exposure time, followed by a gradual recovery of the work per unit indentation volume comparable to that of the un-charged material, despite the variation in the results for S25C.

Fig. 9. Hydrogen content of S25C as a function of exposure time to air.

4. Discussion

The hydrogen content of the test specimens was measured using thermal desorption analysis implemented with a gas chromatograph system (GC-2014, TCD, Shimadzu). The temperature was increased from 40°C to 400°C at 5°C/min and held at that temperature. The dissolved hydrogen concentration was calculated from the total hydrogen content measured during the 4-h measurement period from the start of the temperature increase. **Figure 9** shows the hydrogen content as a function of exposure time to air after hydrogen charging for S25C, where, in a result that confirms that the hydrogen concentration in the material decreases with increasing exposure time to air, the hydrogen concentration goes from 0.43 to 0.17 to essentially zero mass ppm at 0, 24, and 48 h after hydrogen charging, respectively. The hydrogen concentration in S25C was undetectable after 48 h of exposure to air. On the other hand, no hydrogen was detected in Fe-3wt.%Si at 0 h after hydrogen charging; the difference is attributed to the fact that this material is a single-crystal with a bcc structure and has a very high diffusion coefficient. These results show that the transition between hardening and softening observed in Figs. 7 and 8 depends on hydrogen concentration. Even though the hydrogen content is not detected conditions in this study, it clearly shows the hardening and softening behavior. We
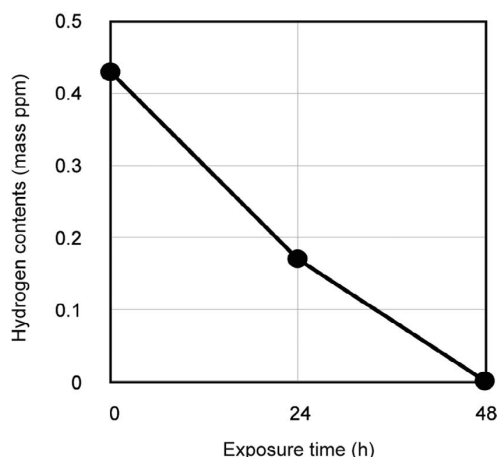
believe those conditions contains less than the detection sensitivity of hydrogen, therefore the softening behavior returns to un-charged state with increasing exposure time. In other words, those materials harden as the hydrogen concentration increases and soften as the hydrogen concentration decreases. When the hydrogen concentration decreases further, the material returns to its original state.

Figure 8 shows that the maximum change in hydrogen-induced work per unit indentation volume is approximately 1×10^9 J/m^3 for both hardening and softening. From Eq. (7), the indented surface area S made by the indenter is:

$$S = \frac{dV}{dh} = 3\beta h^2 \quad \text{..........................} (10)$$

The difference in load per unit indenter area with and without hydrogen (*i.e.*, the difference in indenter stress) can be calculated from Eqs. (5)–(7), (9), and (10) as follows:

$$\frac{\Delta F}{S} = \frac{\left(\alpha_{\text{with H}} - \alpha_{\text{w/o H}}\right) h^{\frac{3}{2}}}{3\beta h^2} = \frac{\frac{5}{2h}\Delta W}{\frac{3V}{h}} = \frac{5}{6}\Delta H \quad \text{.....} (11)$$

Equation (11) shows that the hydrogen-induced work per unit indentation volume (ΔH) is multiplied by 5/6. Therefore, the presence of hydrogen changes the indentation

stress by approximately 0.83 GPa with respect to the no hydrogen charged specimen. From Eqs. (4) and (5), the ratio of the hydrogen-induced load to the indentation load in the absence of hydrogen ($\Delta F/F$) is:

$$\frac{\Delta F}{F} = \frac{\left(\alpha_{\text{with H}} - \alpha_{\text{w/o H}}\right)h^{\frac{3}{2}}}{\alpha_{\text{w/o H}}h^{\frac{3}{2}}} = \frac{\alpha_{\text{with H}}}{\alpha_{\text{w/o H}}} - 1 \quad \text{.......... (12)}$$

Calculating the average value of Eq. (12) at the hydrogen concentration at which maximum softening occurred for S25C and Fe-3wt.%Si are approximately -0.14 and -0.06, respectively. Therefore, the softening detected experimentally can be considered to cause significant differences. Matsumoto's long-time molecular dynamics results predict that at very low dislocation velocities ($<<$ 1 mm/s) the critical resolved shear stress of edge dislocations is almost zero with or without hydrogen,[8] making it unlikely that the presence of hydrogen affects the behavior of edge dislocations in the experimental results. In contrast, the results of Itakura et al.[9] suggest that the mobility of the screw dislocation depends on hydrogen concentration. While research into hydrogen embrittlement mechanisms has extensively investigated hardening at high hydrogen concentrations, the results of the present study reveal significant softening at very low hydrogen concentrations.

Next, we discuss the variations in α with and without hydrogen, considering that plastic deformation during indentation is dictated solely by dislocation motion. According to dislocation theory,[17] the total work W_d due to dislocation sweep is

$$W_d = \tau\left(l\Delta x\right)b \quad \text{............. (13)}$$

where τ is the average shear stress required to move the dislocation, l is the total length of the dislocation line, Δx is the average distance of the dislocation line travelling and b is the magnitude of the Burgers vector. Conversely, the strain rate as a function of dislocation velocity v_d is

$$\dot{\gamma} = \rho b v_d \quad \text{................................. (14)}$$

where

$$\rho = \frac{l}{V_{pl}} \quad \text{................................. (15)}$$

is the dislocation density, with V_{pl} being the volume of the plastic zone. We now simply approximate the geometry of the plastic zone is hemispherical and the indenter is spherical.[18,19] The radius c to the edge of the plastic zone is

$$\frac{c}{R} = \left(\frac{2E}{3\sigma_{ys}}\right)^{\frac{1}{3}} \quad \text{............................. (16)}$$

where σ_{ys} is the yield stress and E is Young's modulus. The volume to the leading edge of the hemispherical plastic zone can be calculated from Eq. (16) and yields

$$\frac{2}{3}\pi c^3 = \left(\frac{2E}{3\sigma_{ys}}\right)\frac{2}{3}\pi R^3 \quad \text{...................... (17)}$$

The volume of the plastic zone is then calculated as follows:

$$V_{pl} = \frac{2}{3}\pi\left(c^3 - R^3\right) = \left(\frac{2E}{3\sigma_{ys}} - 1\right)\frac{2}{3}\pi R^3$$

$$= \left(\frac{2E}{3\sigma_{ys}} - 1\right)V = aV \quad \text{......... (18)}$$

$$a = \left(\frac{2E}{3\sigma_{ys}} - 1\right)$$

where V is the indentation volume. The volume of the plastic zone is expressed as the indentation volume V multiplied by the constant a since Young's modulus and yield stress are intensive material constants. Equation (14) therefore takes the form

$$\dot{\gamma} = \rho b v_d = \frac{lbv_d}{aV} \quad \text{.......................... (19)}$$

which gives

$$V = \frac{lbv_d}{a\dot{\gamma}} \quad \text{................................. (20)}$$

From the above discussion, if the indentation work $W = W_d$, then

$$\frac{W}{V} = \frac{W_d}{V} = \frac{\tau\left(l\Delta x\right)b}{1}\frac{a\dot{\gamma}}{lbv_d} = \tau a\dot{\gamma}\frac{\Delta x}{v_d} \quad \text{........... (21)}$$

where $\Delta x/v_d$ is the average time of dislocation motion, which we assign to the indentation time t_{in} to obtain

$$\frac{W}{V} = \tau a\dot{\gamma}t_{\text{in}} \quad \text{............................. (22)}$$

Given that the indentation time is the same with and without hydrogen, we calculate the difference in work per unit indentation volume with and without hydrogen, which gives

$$\frac{\Delta W}{V} = \left(\tau_{\text{with H}}a_{\text{with H}}\dot{\gamma}_{\text{with H}} - \tau_{\text{w/o H}}a_{\text{w/o H}}\dot{\gamma}_{\text{w/o H}}\right)t_{\text{in}} \quad \text{..... (23)}$$

where the subscript "with H" is for the materials with hydrogen and the subscript "w/o H" is for the materials without hydrogen. Since the volume of the plastic zone is constant [see Eq. (18); Young's modulus and yield stress are almost independent of hydrogen content], a and $\dot{\gamma}$ are also constant. Equation (23) can therefore be expressed as:

$$\frac{\Delta W}{V} = a\dot{\gamma}\left(\tau_{\text{with H}} - \tau_{\text{w/o H}}\right)t_{\text{in}} \quad \text{.................. (24)}$$

Equation (24) gives the hydrogen-induced work per unit indentation volume under simplifying assumptions and is related to the hydrogen-induced work per unit indentation volume in Eq. (9). As opposed to Eq. (9), Eq. (24) does not include a term for the indentation depth h but considers only plastic deformation. Therefore, Eq. (24) indicates that the softening and hardening behavior detected in this study depends strongly on dislocation mobility, as only the shear stress τ, which is necessary for dislocation motion, depends on hydrogen content. As mentioned above, yield stress is essentially independent of hydrogen content because the critical resolved shear stress of the edge dislocations does not depend on hydrogen content, so the dominant effect of hydrogen in this experiment is the shear stress, which is required for the migration of screw dislocations. However,

the dominant factors that dictate the softening or hardening detected by nanoindentation require further investigation, which was revealed when we assumed from Eq. (18) that the volume of the plastic zone is independent of the hydrogen content, whereas observations of crack growth indicate that in the presence of hydrogen the size of the plastic zone decreases,[20] and the associated increase in dislocation density and change in plastic strain rate are considered influential on the softening and hardening behavior. Furthermore, the present results indicate that the hydrogen concentration clearly affects the softening and hardening in the initial state of plastic deformation under indentation and can thus be considered a fundamental part of hydrogen embrittlement, despite the softening and hardening observed in the present nanoindentation tests cannot directly compared with the softening and hardening behavior under tensile stress, this latter being important for crack propagation.

5. Conclusions

This study applied nanoindentation tests to the ferrite-phase bcc-structured polycrystalline carbon steel S25C and single-crystalline Fe-3wt.%Si. Hydrogen-induced work per unit indentation volume was evaluated using uncharged and charged materials exposed for various times in air after hydrogen charging. The hydrogen-induced work per unit indentation volume shows that the specimens harden immediately upon hydrogen charging, then gradually soften with increasing exposure time to air before returning to their original state. This change is attributed to the change in hydrogen concentration. The softening and hardening behavior is considered to attributes the dislocation mobility in the presence of hydrogen. The softening and hardening behavior as a function of hydrogen content identified in the nanoindentation test suggests that the macroscopic mechanical response is quantitatively affected by hydrogen content.

REFERENCES

1) H. Matsui and H. Kimura: *Mater. Sci. Eng.*, **40** (1979), 207. https://doi.org/10.1016/0025-5416(79)90191-5
2) S. Asano and R. Otsuka: *Scr. Metall.*, **1** (1976), 1015. https://doi.org/10.1016/0036-9748(76)90119-8
3) P. J. Ferreira, I. M. Robertson and H. K. Birnbaum: *Acta Mater.*, **46** (1998), 1749. https://doi.org/10.1016/S1359-6454(97)00349-2
4) I. M. Robertson: *Eng. Fract. Mech.*, **68** (2001), 671. https://doi.org/10.1016/S0013-7944(01)00011-X
5) R. Matsumoto and S. Taketomi: *Comput. Mater. Sci.*, **171** (2020), 109240. https://doi.org/10.1016/j.commatsci.2019.109240
6) S. Taketomi, R. Matsumoto and N. Miyazaki: *J. Mater. Res.*, **26** (2011), 1269. https://doi.org/10.1557/jmr.2011.106
7) S. Taketomi, R. Matsumoto and S. Hagihara: *ISIJ Int.*, **57** (2017), 2059. https://doi.org/10.2355/isijinternational.ISIJINT-2017-172
8) R. Matsumoto, S. Oyinbo, M. Vijendran and S. Taketomi: *ISIJ Int.*, **62** (2022), 2402. https://doi.org/10.2355/isijinternational.ISIJINT-2022-311
9) M. Itakura, H. Kaburaki, M. Yamaguchi and T. Okita: *Acta Mater.*, **61** (2013), 6857. https://doi.org/10.1016/j.actamat.2013.07.064
10) N. Nagashima and M. Hayakawa: *J. High Press. Inst. Jpn.*, **51** (2013), 312 (in Japanese). https://doi.org/10.11181/hpi.51.312
11) A. Barnoush and H. Vehoff: *Scr. Mater.*, **55** (2006), 195. https://doi.org/10.1016/j.scriptamat.2006.03.041
12) A. Barnoush and H. Vehoff: *Corros. Sci.*, **50** (2008), 259. https://doi.org/10.1016/j.corsci.2007.05.026
13) A. Barnoush and H. Vehoff: *Acta Mater.*, **58** (2010), 5274. https://doi.org/10.1016/j.actamat.2010.05.057
14) D.-H. Lee, J.-A Lee, M.-Y. Seok, U. B. Baek, S. H. Nahm and J.-I. Jang: *Int. J. Hydrog. Energy*, **39** (2014), 1897. https://doi.org/10.1016/j.ijhydene.2013.11.060
15) K. Tomatsu, T. Omura, Y. Nishiyama and Y. Todaka: *ISIJ Int.*, **56** (2016), 2298. https://doi.org/10.2355/isijinternational.ISIJINT-2016-189
16) Y. Zhao, M.-Y. Seok, I. C. Choi, Y.-H. Lee, S.-J. Park, U. Ramamurty, J.-Y. Suh and J.-I. Jang: *Scr. Mater.*, **107** (2015), 46. https://doi.org/10.1016/j.scriptamat.2015.05.017
17) J. P. Hirth and J. Lothe: Theory of Dislocations, John Wiley & Sons, USA, (1982), 59.
18) R. Hill: The Mathematical Theory of Plasticity, Oxford Press, USA, (1950), 97.
19) M. Mata, O. Casals and J. Alcala: *Int. J. Solids Struct.*, **43** (2006), 5994. https://doi.org/10.1016/j.ijsolstr.2005.07.002
20) S. Aomatsu and R. Matsumoto: *ISIJ Int.*, **54** (2014), 2411. https://doi.org/10.2355/isijinternational.54.2411